Optics Letters

Dual-focus stimulated Raman scattering microscopy: a concept for multi-focus scaling

Sandro Heuke, Barbara Sarri, Alberto Lombardini, Xavier Audier, and Hervé Rigneault*

Aix Marseille Univ, CNRS, Centrale Marseille, Institut Fresnel, Marseille, France
**Corresponding author: herve.rigneault@fresnel.fr*

Received 22 June 2018; revised 28 August 2018; accepted 3 September 2018; posted 4 September 2018 (Doc. ID 335851); published 25 September 2018

High-speed imaging is of the utmost importance for video-rate live cell investigations or to study extended sample areas at sufficient spatial resolution within reasonable time scales. Improving the speed of single-focus stimulated Raman scattering (SRS) microscopy is ultimately restricted by the sample's damage threshold and the shot noise of the demodulated laser source. To overcome this limitation, we present a dual-focus SRS approach modulating the pump laser for each focus at a distinct frequency. The corresponding probe beams are detected each by a photodiode and demodulated individually by two separate lock-in units to avoid inter-focal cross-talk. Two laterally or axially displaced images as well as hyperspectral SRS images can be obtained simultaneously within the field of view of the objective lens. The modular implementation presented here can be extended to multiple foci by using multi-channel acousto-optics modulators in combination with multi-channel lock-in amplifiers.

OCIS codes: (180.4315) Nonlinear microscopy; (290.5910) Scattering, stimulated Raman; (170.6935) Tissue characterization.

https://doi.org/10.1364/OL.43.004763

Since the first half of the past century, state-of-the-art cancer diagnosis has been based on various staining protocols of excised tissue [1]. Depending on the degree of dyspepsia and type of surgery, e.g., biopsy or full tumor resection, the diameter of tissue blocks removed may vary from sub-millimeter to several centimeters. Slicing the latter in steps of 5–15 μm results in a few or up to several hundred tissue sections that will be evaluated by a trained pathologist. Standard methods such as the haematoxylin and eosin (H&E) staining protocol are very efficient with capacities to color several hundred sections of nearly arbitrary size at once within about 20 min. Nevertheless, the whole procedure covering the freezing, cutting, and staining of tissue sections, plus human evaluation is time consuming, requiring between 1 h for a frozen section analysis up to several days for embedded tissue blocks. Thus, the development of faster and more efficient diagnostic *in* or *ex vivo* procedures is desirable. Recent progress in nonlinear optical imaging suggests that stimulated Raman scattering (SRS) microscopy can be used to generate virtual H&E images—accessing the same information content as conventional protocols—without staining the sample [2,3]. For diagnostic purposes, sub-cellular resolution, i.e., a minimum of 1 μm inter-pixel distance, is required. For a single square sample of 1 cm length and assuming best image acquisition times of 100-10 μs per pixel, the total duration until diagnosis lasts between 3 h and 15 min. Consequently, the current technological state requires an improvement of at least a factor of 10-100 in image acquisition velocity to become comparable or eventually outperform chemical-staining technology. Improvement of single-focus SRS acquisition time is limited, however, by the sample's damage threshold and the shot noise of the laser source [4]. As both factors are already well optimized using infrared excitation and low noise solid-state laser sources modulated at half the lasers' repetition rate [5], multiplexing of the image acquisition becomes the method of choice. Wide-field SRS microscopy would require cameras with extended photon-to-charge conversion capacities [6] and read-out frequencies above high levels of flicker noise of the demodulated laser source, i.e., above 1 MHz [7]. Yet, these kinds of cameras are not commercially available. Alternatively, multi-focus approaches may offer a second opportunity to increase imaging velocity by parallelization of the acquisition from different spatial regions of the sample [8]. Approaches such as disk scanning or time-multiplexed detection [9,10], used in other optical microscopy techniques, are not compatible with SRS imaging, where high photo-currents at MHz detection frequency have to be analyzed. Thus, single-element detection combined with a suitable way to distinguish the contribution of different foci seems to be an appropriate path.

Here, we present an approach that uses two acousto-optic modulators (AOMs) to imprint different modulation frequencies on two separately guided pump beams. The latter are superimposed with Stokes beams and directed toward laser-scanning mirrors with a distinct angle of incidence. The objective lens translates this angular difference into foci of displaced lateral positions at the sample. Separation of individual image content is achieved by dividing the beams using a mirror or a polarizing beam splitter. To avoid inter-focal cross-talk as well as to achieve an effective improvement of the overall signal to noise (S/N), the Stokes beams are detected individually by two photodiodes (PDs) connected to separate lock-in amplifiers.

The implementation of the dual-focus SRS configuration is presented in Fig. 1. Two optical parametric oscillators (OPOs, APE Emerald) are pumped at 515.5 nm by a frequency-doubled Yb-fiber laser (APE Emerald engine, 80 MHz, 2–3 ps) that, in addition, generates 1031 nm serving directly as Stokes for both foci. Matching molecular vibrations from 500 cm^{-1} to 5000 cm^{-1}, the OPOs' emission can be tuned independently from 680 nm to 980 nm. The output of each OPO is modulated separately at distinct frequencies at 19.9 MHz and 20 MHz using AOMs (AA, MT200-B100A0,5-800). Note that the selection of modulation frequencies is of minor importance and could have been chosen to range from 10 MHz to 25 MHz with a cross-talk free $\Delta f > 0.05$ MHz for our experimental configuration and parameters. The pump and Stokes beams are temporally and spatially superimposed by means of a 50:50 beam splitter, two dichroics, and delay stages. Note that a second OPO is actually not necessary, as the output of the first could be split and modulated at different frequencies, but benefits here an extra amount of power and freedom for wavelength tuning for a hyper-spectral imaging application. The joined beams are coupled into a home-built laser-scanning SRS microscope [11] but feature a different angle of incidence at the laser-scanning mirrors. Using a 20× objective [Nikon, CFI PLAN APO LBDA, numerical aperature (NA) = 0.75, immersion: air], the angle difference translates into a lateral displacement of the foci at the sample. The power at the focal plan is approximately 20 mW for each beam. A 60× objective (Nikon, Fluor, NA = 1, immersion: water) is used to collect the laser beams in forward direction. Wavelengths below 1000 nm are blocked by suitable dielectric filters, while the two Stokes beams corresponding to the different foci are separated by means of a silver mirror or a polarizing beam splitter and centered onto two independent PDs (APE). For each PD, the signal is demodulated by two individual lock-in-amplifiers (APE and Zurich Instruments, HF2LI) at distinct modulation frequencies to avoid cross-talk between channels that might result from scattering or polarization rotation when using the same modulation frequency. It is noted that the excess noise level of the Yb-fiber laser was measured to be 6 dB(V) ≈ 3 dB(V) at 20 MHz, meaning that a similar image quality as in Figs. 2–5 could have been obtained within 1/4 of the acquisition time (see figure captions) using a purely shot-noise-limited system.

At first glance, it may seem advantageous to detect both Stokes beams by a single PD, split its output, and connect it to both lock-in amplifiers. Such a procedure will simplify the setup for some applications but will not add to the desired improvement of the overall image acquisition velocity as readily outlined. Assume that a certain minimum S/N ratio of an SRS image is achieved using a single focus. The addition of n other foci modulated at different frequencies f_n will gain n further images but increase the noise at each demodulated frequency by a factor of $\sqrt{n}$ as a result of the elevated shot noise arising from n times more power at the PD. To compensate for the raised noise level, every image has to be averaged $(\sqrt{n})^2 = n$ times longer. n times more images with a sufficient S/N oppose a n times longer acquisition time. Consequently, no acceleration is achieved, and the contribution for individual foci, therefore, have to be detected separately. Note that the same argument will encumber any potential single-pixel camera SRS approach.

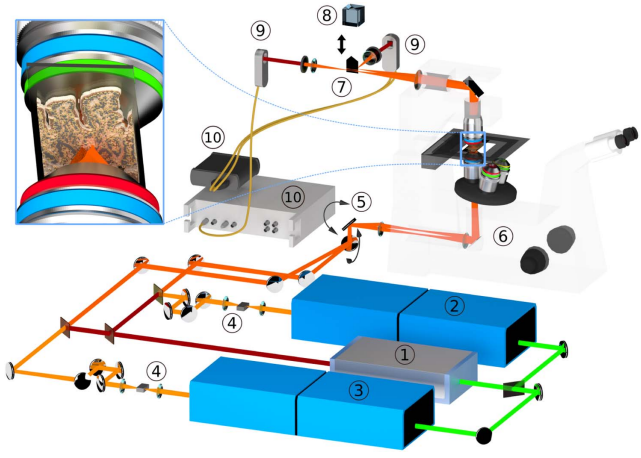

Fig. 1. Experimental implementation of the dual-focus SRS approach: ① Yb-fiber laser, ② OPO1, ③ OPO2, ④ AOM, ⑤ laser-scanning mirrors, ⑥ laser-scanning microscope, ⑦ edge-mirror, ⑧ polarizing beam splitter, ⑨ photodiodes, ⑩ lock-in amplifiers. The zoom displays the spatially separated focusing of the excitation beams.

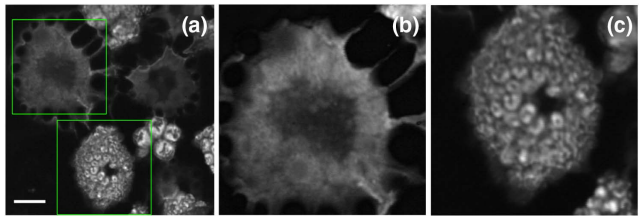

Fig. 2. Dual-focus SRS images of adipocytes: (a) overview image displaying several cells at 2850 cm^{-1}. (b) and (c) Zoom of image (a) acquired simultaneously by shifting the focal center position of each focus to the middle of the cell under investigation. The images were separated using a mirror (see also Fig. 1). Scale bar equals 30 µm. Image parameters: pixel dwell time: 160 µs, resolution: (a) 400 × 400, (b) and (c) 300 × 300, acquisition time: (a) 26 s, (b) plus (c) 15 s.

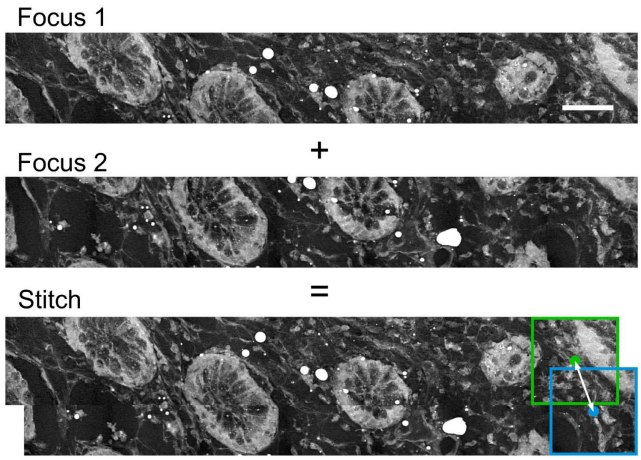

Fig. 3. Splitting the field of view in SRS imaging. Two adjacent sequences of images were acquired by adjusting the size of the investigated area and interfocal distance to reduce the acquisition time per area scanned. The blue and green boxes outline individual images of different foci. Scale bar: 50 µm. Image parameters: pixel dwell time: 200 µs, resolution: 200 × 1400, acquisition time: 1 min.

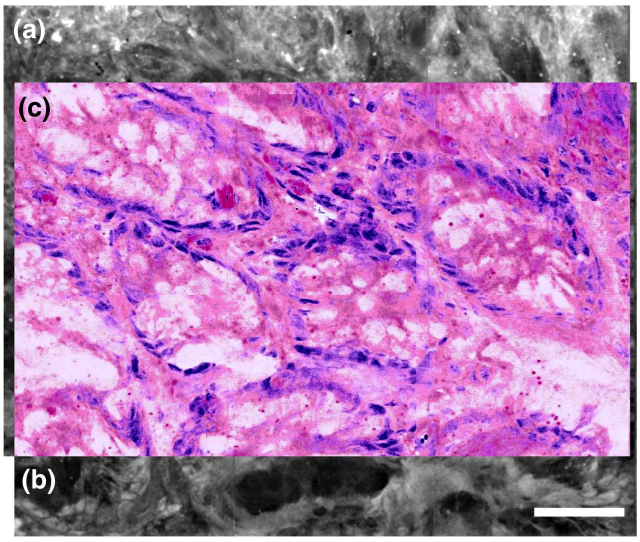

Fig. 4. Hyperspectral SRS imaging. OPO1 and OPO2 were tuned to match 2850 cm^{-1} (a) and 2930 cm^{-1} (b), respectively. The foci are approximately 10 μm displaced to split sufficiently the thermal energy dissipated into the tissue. Using both SRS images, a virtual H&E-stained image (c) can be generated. Note that parts of the upper and lower overlapping areas were not converted into a virtual H&E image to display native data. Scale bar: 100 μm. Image parameters: pixel dwell time: 160 μs, resolution: (c) 410 × 680, acquisition time: 45 s.

We employ two different methods for separation of the Stokes beams: using either different mirrors at the Fourier plane of the sample or a polarizing beam splitter. These methods are self-sufficient for a dual-focus scheme, but their combination is required for a general multi-focus application, where a line of laterally scanned foci with alternating states of polarization might be used. Following this suggestion would circumvent the limitation of the missing overlap of adjacent images of the mirror approach while more than two foci can be employed as for the implementation of the polarizing beam splitter. As the first application of a dual-focus approach, Fig. 2 displays SRS images at a Raman resonance of 2850 cm^{-1} of a culture of lipid-rich adipocytes at different development stages. Real-time imaging of the adipocytes and their progenitors is of interest, as they are found to play an important role in several processes, e.g., signaling and modulating of organ regeneration or supply of nutritional and metabolic functions in mammary glands [12]. If several cells are imaged over a period of time, e.g., to follow their development during the maturation process, it is advantageous to acquire two or several images containing only highly spatially resolved information about the cells rather than to lose time while imaging the empty space in between.

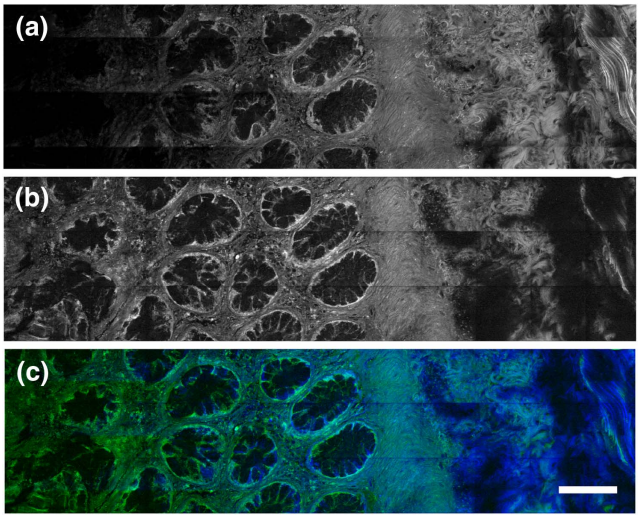

Fig. 5. SRS imaging at distinct depths of a human colon sample. By changing the divergence of one beam pair, the foci are axially displaced. The subfigures (a) and (b) display SRS images at depth differences of approximately 5 μm. Subfigure (c) outlines the superposition of figure (a) and (b) in false color blue and green, respectively. Scale bar: 100 μm. Image parameters: pixel dwell time: 200 μs, resolution: (c) 600 × 2300, acquisition time: 280 s.

Figure 3 displays two SRS images at 2930 cm^{-1} of a thin section of human colon tissue that were acquired simultaneously using approximately 50 μm laterally displaced foci. The maximum possible foci displacement is comparable to the size of the field of view (FOV) for a single SRS image with an added opportunity to optimize the overlap of the pump and Stokes beams for a segment of the objective lens' FOV. As both images share an overlap, a seamless stitching procedure can be applied to smooth the transition from one image to the other if necessary [13,14]. The size of the overlap is readily adjusted by changing the angle of the incoming beams or by modifying the extent of the scanned area for an individual image. Thus, without compromising the image quality, the overall image acquisition time can almost be divided in half.

The third application outlined in Fig. 4 concerns hyperspectral imaging with approximately 10 μm lateral displaced foci. For demonstration, OPO1 was tuned at 2850 cm^{-1} and OPO2 to 2930 cm^{-1} to image the lipid and protein content of a human colon sample that is readily translated into a virtual-H&E image highlighting the position, size, and density of nuclei. To obtain such an artificial H&E image, the SRS-image at 2850 cm^{-1} is subtracted from that at 2930 cm^{-1}, false-color coded in purple, and superimposed with the original SRS image at 2850 cm^{-1} color-coded in rose. As an advantage over single-focus dual-frequency SRS [15–20] the excitation power of the pump beams is split over two locations. Thus, either less photo-damage is introduced or—by increasing the power per foci—more signal per Raman resonance can be obtained without damaging the sample.

For the third application, recall that in histopathology, extended areas of certain millimeters width with an axial extension of a few micrometers have to be investigated. If the sample is tilted with respect to the optical table by only about 1° and the sample is laterally displaced by 1 mm, e.g., by means of a translational stage, the axial focus position will have shifted about 17 μm, i.e., be outside the tissue section. Thus, a second focus may become useful at another depth of the sample, which was achieved here by the introduction of a lens with $f =$ 200 cm for one probe and Stokes pair just before the laser-scanning mirrors. Figures 5(a) and 5(b) display SRS images generated at different focal depths of a human colon sample acquired at a Raman shift of 2930 cm^{-1}. A weighted summation of both images, e.g., linear or taking the brighter image, can be used to restore the image of the tilted sample.

Scaling of the approach to generate a multi-focus SRS system requires additional laser power, multi-channel lock-in

amplifiers, as well as multi-channel AOMs, which are all commercially available. As every focus is cross-talk free when detected by an individual combination of a PD and lock-in amplifier, the addition of n foci results in a n times faster image acquisition for a given FOV. The design of a mirror element for multi-beam separation may be inspired by the architecture of prism arrays used to reorganize the propagation structure of laser diode arrays [21]. Alternatively, PD arrays of suitable geometries would have to be created.

In conclusion, we demonstrated dual-focus SRS microscopy as the first concept that allows to multiplex the position of data acquisition. The introduction of this concept is of particular importance for all histological SRS microscopy application, as it opens up a path to bypass the ultimate speed limitation, i.e., detection shot noise, of a single focus. Thus, it enables all forthcoming developments in SRS microscopy to become applicable for almost arbitrary sample sizes, i.e., builds the theoretical bridge from a lab experiment to a time-optimized routine application after up-scaling of the foci number.

Funding. Centre National de la Recherche Scientifique (CNRS); Aix-Marseille University A*Midex (ANR-11-IDEX-0001-02); Agence Nationale de la Recherche (ANR) grants France Bio Imaging (ANR-10-INSB-04-01); France Life Imaging (ANR-11-INSB-0006) infrastructure networks; Plan cancer INSERM (PC201508).

Acknowledgment. We thank Olivier Piot and Valérie Untereiner from Reims University for providing us with the adipocytes.

REFERENCES

1. M. Titford, Biotech. Histochem. **80**, 73 (2005).
2. F.-K. Lu, D. Calligaris, O. I. Olubiyi, I. Norton, W. Yang, S. Santagata, X. S. Xie, A. J. Golby, and N. Y. R. Agar, Cancer Res. **76**, 3451 (2016).
3. D. A. Orringer, B. Pandian, Y. S. Niknafs, T. C. Hollon, J. Boyle, S. Lewis, M. Garrard, S. L. Hervey-Jumper, H. J. L. Garton, C. O. Maher, J. A. Heth, O. Sagher, D. A. Wilkinson, M. Snuderl, S. Venneti, S. H. Ramkissoon, K. A. McFadden, A. Fisher-Hubbard, A. P. Lieberman, T. D. Johnson, X. S. Xie, J. K. Trautman, C. W. Freudiger, and S. Camelo-Piragua, Nat. Biomed. Eng. **1**, 0027 (2017).
4. Y. Ozeki, F. Dake, S. Kajiyama, K. Fukui, and K. Itoh, Opt. Express **17**, 3651 (2009).
5. Y. Ozeki, Y. Kitagawa, K. Sumimura, N. Nishizawa, W. Umemura, S. Kajiyama, K. Fukui, and K. Itoh, Opt. Express **18**, 13708 (2010).
6. B. Marx, L. Czerwinski, R. Light, M. Somekh, and P. Gilch, J. Raman Spectrosc. **45**, 521 (2014).
7. K. Mars, D. X. Lioe, S. Kawahito, K. Yasutomi, K. Kagawa, T. Yamada, and M. Hashimoto, Sensors **17**, 2581 (2017).
8. E. E. Hoover and J. A. Squier, Nat. Photonics **7**, 93 (2013).
9. S. Heuke, F. B. Legesse, A. Lorenz, T. Pascher, D. Akimov, M. Jäger, M. Schmitt, and J. Popp, Opt. Lett. **40**, 2505 (2015).
10. F. B. Legesse, T. Meyer, S. Heuke, T. Gottschall, T. Pascher, J. Limpert, A. Tünnermann, M. Schmitt, and J. Popp, Opt. Lett. **42**, 183 (2017).
11. S. Brustlein, P. Ferrand, N. Walther, S. Brasselet, C. Billaudeau, D. Marguet, and H. Rigneault, J. Biomed. Opt. **16**, 021106 (2011).
12. R. K. Zwick, C. F. Guerrero-Juarez, V. Horsley, and M. V. Plikus, Cell Metab. **27**, 68 (2018).
13. F. Legesse, O. Chernavskaia, S. Heuke, T. Bocklitz, T. Meyer, J. Popp, and R. Heintzmann, J. Microsc. **258**, 223 (2015).
14. O. Chernavskaia, S. Guo, T. Meyer, N. Vogler, D. Akimov, S. Heuke, R. Heintzmann, T. Bocklitz, and J. Popp, J. Chemom. **31**, e2901 (2017).
15. E. Ploetz, S. Laimgruber, S. Berner, W. Zinth, and P. Gilch, Appl. Phys. B **87**, 389 (2007).
16. D. Zhang, M. N. Slipchenko, D. E. Leaird, A. M. Weiner, and J.-X. Cheng, Opt. Express **21**, 13864 (2013).
17. R. He, Y. Xu, L. Zhang, S. Ma, X. Wang, D. Ye, and M. Ji, Optica **4**, 44 (2016).
18. X. Audier, N. Balla, and H. Rigneault, Opt. Lett. **42**, 294 (2017).
19. C.-S. Liao, P. Wang, P. Wang, J. Li, H. J. Lee, G. Eakins, and J.-X. Cheng, Sci. Adv. **1**, e1500738 (2015).
20. S. Heuke, B. Sarri, X. Audier, and H. Rigneault, Opt. Lett. **43**, 3582 (2018).
21. Z. Huang, L. Xiong, H. Liu, Z. Wang, P. Zhang, Z. Nie, D. Wu, and X. Liu, Opt. Eng. **52**, 106108 (2013).